



# Identification and Tracking of Alloreactive T Cell Clones in Rhesus Macaques Through the RM-scTCR-Seq Platform

Ulrike Gerdemann<sup>1†</sup>, Ryan A. Fleming<sup>1†</sup>, James Kaminski<sup>1,2,3,4†</sup>, Connor McGuckin<sup>1</sup>, Xianliang Rui<sup>1</sup>, Jennifer F. Lane<sup>1</sup>, Paula Keskula<sup>1</sup>, Lorenzo Cagnin<sup>1</sup>, Alex K. Shalek<sup>2,3,4‡</sup>, Victor Tkachev<sup>1‡</sup> and Leslie S. Kean<sup>1\*‡</sup>

## OPEN ACCESS

### Edited by:

Jianing Fu,  
Columbia University, United States

### Reviewed by:

Adam Griesemer,  
Columbia University, United States

Gerald Morris,

University of California, San Diego,  
United States

### \*Correspondence:

Leslie S. Kean  
leslie.kean@childrens.harvard.edu

<sup>†</sup>These authors have contributed  
equally to this work and share  
first authorship

<sup>‡</sup>These authors have contributed  
equally to this work and share  
last authorship

### Specialty section:

This article was submitted to  
Alloimmunity and Transplantation,  
a section of the journal  
Frontiers in Immunology

Received: 29 October 2021

Accepted: 22 December 2021

Published: 26 January 2022

### Citation:

Gerdemann U, Fleming RA,  
Kaminski J, McGuckin C, Rui X,  
Lane JF, Keskula P, Cagnin L,  
Shalek AK, Tkachev V and Kean LS  
(2022) Identification and  
Tracking of Alloreactive T Cell  
Clones in Rhesus Macaques Through  
the RM-scTCR-Seq Platform.  
*Front. Immunol.* 12:804932.  
doi: 10.3389/fimmu.2021.804932

<sup>1</sup> Division of Pediatric Hematology/Oncology, Boston Children's Hospital; Department of Pediatric Oncology, Dana Farber Cancer Institute and Harvard Medical School, Boston, MA, United States, <sup>2</sup> Broad Institute of MIT and Harvard, Cambridge, MA, United States, <sup>3</sup> Department of Chemistry, Institute for Medical Engineering and Science (IMES), and Koch Institute for Integrative Cancer Research, MIT, Cambridge, MA, United States, <sup>4</sup> Ragon Institute of Massachusetts General Hospital (MGH), MIT and Harvard, Cambridge, MA, United States

T cell receptor (TCR) clonotype tracking is a powerful tool for interrogating T cell mediated immune processes. New methods to pair a single cell's transcriptional program with its TCR identity allow monitoring of T cell clonotype-specific transcriptional dynamics. While these technologies have been available for human and mouse T cells studies, they have not been developed for Rhesus Macaques (RM), a critical translational organism for autoimmune diseases, vaccine development and transplantation. We describe a new pipeline, 'RM-scTCR-Seq', which, for the first time, enables RM specific single cell TCR amplification, reconstruction and pairing of RM TCR's with their transcriptional profiles. We apply this method to a RM model of GVHD, and identify and track *in vitro* detected alloreactive clonotypes in GVHD target organs and explore their GVHD driven cytotoxic T cell signature. This novel, state-of-the-art platform fundamentally advances the utility of RM to study protective and pathogenic T cell responses.

**Keywords:** TCR sequencing, single cell sequencing, alloreactive T cells, Rhesus Macaque (*Macaca mulatta*), GVHD

## INTRODUCTION

Expression of the highly polymorphic (up to  $10^{18}$  specificities) (1) T cell receptor (TCR) allows T cells to specifically recognize foreign and self-antigens presented in the context of the Major Histocompatibility Complex (MHC) by antigen presenting cells. This diversity is achieved by complex genetic recombination of the T cell alpha and beta chain during thymic T cell development, and results in a unique molecular barcode for each T cell. These unique TCR sequences enable studies of clonal- and diversity- dynamics in models of transplantation, infection, tumor immunology and vaccine development (2–7). More recently TCR tracking has been combined with high throughput single cell RNA sequencing (scRNA-Seq), enabling transcriptional profiling of distinct T cell clonotypes within and across samples (8, 9).

To date, clonotype tracking technologies have been developed for both mouse and human TCRs, facilitating studies of T cell clonal dynamics at an unprecedented level of molecular sensitivity (9–11). However, both murine and human models have drawbacks: The inbred nature of mice and the evolutionary distance between the murine and human immune systems can restrict the clinical applicability of murine results. Moreover, the study of human single cell TCR data continues to focus predominantly on the peripheral blood, being restricted by inherent challenges in accessing human tissues during health and disease. This can result in an incomplete picture of important immunological processes when using human samples.

To address these limitations, nonhuman primate (NHP) models (particularly using rhesus macaques (RM)) have been essential (12), and have enabled critical advances for some of the most pressing human needs, including the development of vaccines against SARS-CoV-2 (13–17), the study of HIV pathogenesis (18–20), and in advancing our mechanistic understanding of solid organ transplant (21, 22) and hematopoietic stem cell transplant (HCT) (23–29). For HCT, NHP models have enabled the translation of several novel therapeutic strategies to the clinic for the prevention of graft-versus-host disease (GVHD), the major cause of transplant-related mortality after HCT (30, 31).

The identification and tracking of TCR clonotypes are of critical importance for each of the clinical settings described above, in order to understand the molecular mechanisms driving immune protection or disease pathogenesis. For acute GVHD (aGVHD), dissecting the link between T cell clonal architecture and disease is particularly relevant, given that donor-derived alloreactive T cells are the main culprits in the aGVHD-mediated destruction of the skin, intestine, and liver (32–34). Accurate identification and characterization of alloreactive T cell clonotypes is essential to identifying the molecular drivers of aGVHD, and doing so in aGVHD-target tissues as well as the peripheral blood remains a major challenge. Until the work described in this manuscript, the identification and tracking of individual TCR clonotypes in NHP models (in particular, RM) has been limited by a lack of robust methodology for single cell TCR sequencing adapted to this essential pre-clinical model. The key limitations facing the field were the lack of effective RM-specific primers that could successfully amplify the TCR region in a highly multiplexed fashion, as well as the incomplete annotation of the RM genome throughout the TCR alpha and beta chain region, which created a major barrier to accurate TCR chain reconstruction.

We now describe the design and validation of RM-specific primers compatible with the human 10x Genomics single cell sequencing platform, which accurately amplifies the RM TCR alpha and beta regions. Amplified fragments aligned to our custom-assembled and annotated RM TCR reference permit, for the first time, the *in vitro* and *in vivo* identification and tracking of RM derived T cell clonotypes. Pairing of *in vivo* identified alloreactive clonotypes with their transcriptional profile revealed a highly activated cytotoxic CD8 T cell signature during NHP aGVHD.

## METHODS

### NHP

This study was conducted in strict accordance with (USDA) United States Department of Agriculture regulations and the recommendations in the Guide for the Care and Use of Laboratory Animals of the National Institutes of Health. It was approved by the Massachusetts General Hospital and Biomere Animal Care and Use Committees. T cells were obtained from healthy colony RM or from animals who underwent allogeneic HCT in the setting of previously published studies (28).

### Mixed Lymphocyte Reaction (MLR)

RM PBMCs were isolated from whole blood by Ficoll gradient centrifugation, and then used for MLR assays either immediately, or after liquid nitrogen cryopreservation in 10% dimethyl sulfoxide (DMSO)/90% fetal bovine serum (FBS). At the time of the MLR, stimulator PBMCs were irradiated with 3500 cGy of (<sup>137</sup>Cs) radiation. Responder PBMCs were stained with cell trace violet (CTV, Invitrogen) as per manufacturer's instructions. 2×10<sup>5</sup> T cell-enriched responder PBMCs along with an equal number of stimulator PBMCs were added to each well in a 96-well plate (Corning) in X-vivo-15 medium (BioWhittaker) supplemented with 10% FBS (Irvine Scientific) and incubated at 37°C for a total of 5 days. Cell culture media change was performed on day 3 of the culture. At the end of 5 days, cells were stained with an extracellular antibody for CD3 (clone SP34-2), CD20 (clone 2H7) and CD14 (clone M5E2, all antibodies from BD Bioscience) for 20min at 4°C, and high-, medium- and non-proliferating CD3+ T cells (identified based on the dilution of CTV) were sorted and processed for single cell sequencing using the Chromium Next GEM Single Cell 5' Reagent Kit v1 with optimized RM primers as described below.

### NHP HCT, Necropsy and Tissue Processing

RM HCT, necropsy, and tissue processing were performed as previously described (28, 31). Single cell suspensions resulting from tissue processing were sorted on a live CD3+ and CD14/CD20- population and prepared for single cell sequencing.

### Sample Processing, Primer Design and PCR Amplification

All products used in the preparation of these samples, excluding the custom primer set designed and described herein, are available from 10x Genomics. While samples in this publication were prepared using the Next GEM 5' v2 Gel Beads with the i7 Multiplex Plate (Single Index), we also validated primers and PCR conditions compatible with the newer Next GEM Single Cell 5' v2 Sample Index Plate TT (Dual Index) (see below).

Single Cell V(D)J v1: GEMs were generated using v2 Gel Beads and the v1 Target Enrichment kit substituting the custom primers for the off-the-shelf human/mouse T Cell Mix 1 and 2 premixed primers. Sample Indexing was performed using the i7 Multiplex Kit plate (10x Genomics, PN-120262). TCR alpha and beta primers were designed to perform in a nested PCR approach

to optimize target enrichment of the respective constant regions (Table 1). TRAC inner and outer primers were 297bp apart, and the beta chain inner and outer primers were 357bp apart. Primers were optimized to match the melting temperature of the 10x v1 forward primers for annealing to a known sequence within the gel beads in emulsion (GEMs) according to the human 10x Genomics Chromium Single Cell V(D)J Reagent Kits User Guide for target enrichment ([https://assets.ctfassets.net/an68im79xiti/31W4aZOJ8C2ipxzTrcQIWn/72c5c2bc3dd7784f44f5218ca345ce04/CG000086\\_ChromiumSingleCellV\\_D\\_J\\_ReagentKits\\_UG\\_RevM.pdf](https://assets.ctfassets.net/an68im79xiti/31W4aZOJ8C2ipxzTrcQIWn/72c5c2bc3dd7784f44f5218ca345ce04/CG000086_ChromiumSingleCellV_D_J_ReagentKits_UG_RevM.pdf)). Primer sequences are listed in Table 1.

PCR was performed with an initial denaturation temperature of 98°C for 45 seconds, followed by denaturation at 98°C for 20 seconds. Annealing was optimal at 67°C for 30 seconds with extension of 72°C for 1 min. A total of 20 PCR cycles were performed with a final extension step at 72°C for 1 min.

Next GEM Single Cell 5' v2: GEMs were also generated using v2 reagent kits for GEM generation and library preparation while substituting the custom RM primers for the off-the-shelf human/mouse T Cell Mix 1 and 2 premixed primers. Sample Indexing was performed using the Dual Index Kit TT (10x Genomics PN-1000215). Primers (Table 2) were optimized to match the melting temperature of the 10x v2 forward primers for annealing to a known sequence within the gel beads in emulsion (GEMs) according to the human 10x Genomics Chromium Single Cell V(D)J Reagent Kits User Guide for target enrichment ([https://assets.ctfassets.net/an68im79xiti/57JaTECQNBSPyDz8oucdi/92da9f62521ea1f5c781ba234bd0a0f5/CG000331\\_ChromiumNextGEMSingleCell5-v2\\_UserGuide\\_RevC.pdf](https://assets.ctfassets.net/an68im79xiti/57JaTECQNBSPyDz8oucdi/92da9f62521ea1f5c781ba234bd0a0f5/CG000331_ChromiumNextGEMSingleCell5-v2_UserGuide_RevC.pdf)). TRAC inner and outer primers were 2996bp apart, and the beta chain inner and outer primers were 354bp apart. Primer sequences are listed in Table 2.

PCR was performed with an initial denaturation temperature of 98°C for 45 seconds, followed by denaturation at 98°C for 20

seconds. Annealing was optimal at 62°C for 30 seconds with extension of 72°C for 1 min. A total of 20 PCR cycles were performed with a final extension step at 72°C for 1 min. Sequencing results utilizing v2 primers are listed in Table S1.

## Reference Transcriptome

The reference transcriptome (Data S4) was created using Cellranger version 6.0.0 with the following steps:

1. We first filtered Ensembl's gtf file for v104 of the macaca mulatta gene annotation using cellranger's mkgtf command with the following attributes:

```
-attribute=gene_biotype:protein_coding -attribute=
gene_biotype:lincRNA -attribute=gene_biotype:miRNA -
attribute=gene_biotype:antisense -attribute=gene_biotype:
IG_LV_gene -attribute=gene_biotype:IG_V_gene -attribute=
gene_biotype:IG_V_pseudogene -attribute=gene_biotype:
IG_D_gene -attribute=gene_biotype:IG_J_gene -attribute=
gene_biotype:IG_J_pseudogene -attribute=gene_biotype:
IG_C_gene -attribute=gene_biotype:IG_C_pseudogene -
attribute=gene_biotype:TR_V_gene -attribute=gene_biotype:
TR_V_pseudogene -attribute=gene_biotype:TR_D_gene -
attribute=gene_biotype:TR_J_gene -attribute=gene_biotype:
TR_J_pseudogene -attribute=gene_biotype:TR_C_gene
```

2. We next edited cellranger's mkref program to use more than one thread using the command:

```
sed -i '88s/num_threads/#num_threads/'/cellranger-6.0.0/
bin/rna/mkref
```

3. We then created the reference transcriptome using cellranger's mkref command: cellranger-6.0.0/bin/rna/mkref -genome=MMulatta\_Ensembl\_v104 -fasta=MMulatta\_Ensembl\_v104\_combined.fasta -genes=MMulatta\_Ensembl\_v104\_combined\_filtered.gtf -nthreads=32 -memgb=128

## VDJ Reference

1. We used version 6.0.2 of Cellranger to create the initial VDJ reference based on IMGT (35, 36).

2. We used the following command to generate the initial reference: cellranger-6.0.2/lib/bin/fetch-imgt -genome vdj\_IMGt\_rhesus -species "Macaca mulatta".

3. This version of the VDJ reference did not include constant regions, so we added the following sequences - obtained from IMGT and Ensembl - to the reference:

```
>340|TRAC*01 IMGT|TRAC|C-REGION|TR|TRA|None|01
ATATCCAGAACCCTGACCCTGCCGTGTACCAGC
TGAGAGGCTCTAAATCCAATGACACCTC
TGTCTGCCTATTTACTGATTTTGATTCTGTAAT
GAATGTGTACAAAGCAAGGATTCTGACGTGCAT
ATCACAGACAAAACCTGTGCTAGACATGAGGTCTATG
GACTTTAAGAGCAACGGTGTGCTGGCCTGGAGCAACAA
ATCCGATTTTGCATGTACAAGCGCCTCAAGGACAG
CGTTATCCAGCAGACACCTTCTTCCCCGGCACAGAA
AGTGTCTGTGATGCCAACCTGGTTGAGAAAAGCTTTG
AAACAGATATGAACCTAAACTTTCAAAACCTGTGAG
TGATTGGGTTCCGAATCCTCCTCTGAAAGTGCCG
GGTTTAATCTGCTCATGACGCTGCGGCTGTGGTC
CAGCTGA
```

TABLE 1 | Primer sequences optimized for RM-scTCR-Seq v1.

Primer	Sequence
Forward Primer 1 (10x Genomics)	AATGATACGGCGACCACCGAGA-TCTACACTCTTTCCCTACACGACGCTC
Forward Primer 2 (10x Genomics)	AATGATACGGCGACCACCGAGA-TCT
Alpha Outer Primer	CGGGCCACTTTCAGGAGGAGG
Alpha Inner Primer	TGTTCTGTGATATGCACGTCAGAA
Beta Outer Primer	CCCCACTCACCTGCTCTACC
Beta Inner Primer	CTCAAACACAGCGACCTTGGGTGG

TABLE 2 | Primer sequences optimized for RM-scTCR-Seq v2.

Primer	Sequence
Forward Primer 1 (10x Genomics)	GATCTACACTCTTTCCCTACACGACGCG
Forward Primer 2 (10x Genomics)	GATCTACACTCTTTCCCTACACGACGCG
Alpha Inner Primer	TGTTCTGTGATATGCACGTCAGAA
Alpha Outer Primer	CGGGCCACTTTCAGGAGGAGG
Beta Inner Primer	TCAAACACAGCGACCTTGGG
Beta Outer Primer	CCCCACTCACCTGCTCTACC

>341|TRAC\*02 TRAC\_205\_Ensembl\_CDS|TRAC|C-REGION|TR|TRA|None|02

ATGAATGTGTCACAAAGCAAGGATTCTGACGTGCAT  
ATCACAGACAAAACCTGTGCTAGACATGAGGTCTATG  
GACTTTAAGAGCAACGGTGTGCTGGCCTGGAGCAAC  
AAATCCAATTTTGCATGTACAAGCGCCTTCAAGGAC  
AGCGTTATTCCAGCAGACACCTTCTTCCCCGGCACAG  
AAAGTGTCTGTGATGCCAACCTGGTTGAGAAAAGCTT  
TGAAACAGATATGAACCTAAACTTTCAAAACCTGTCA  
GTGATTGGGTTCCGAATCCTCCTCCTGAAAGTGGCC  
GGGTTAATCTGCTCATGACGCTGCGGCTGTGGTC  
CAGCTGA

>342|TRAC\*03 TRAC\_201\_Ensembl\_CDS|TRAC|C-REGION|TR|TRA|None|03

ATGAATGTGTCACAAAGCAAGGATTCTGACGTGCAT  
ATCACAGACAAAACCTGTGCTAGACATGAGGTCTATG  
GACTTTAAGAGCAACGGTGTGCTGGCCTGGAGCAAC  
AAATCCAATTTTGCATGTACAAGCGCCTTCAAGGACA  
GCGTTATTCCAGCAGACACCTTCTTCCCCGGCACAG  
AAAGTGTCTGTGATGCCAACCTGGTTGAGAAAAGC  
TTTGAACAGATATGAACCTAAACTTTCAAAACCTG  
TCAGTGATTGGGTTCCGAATCCTCCTCCTGAAAGTG  
GCCGGGTTAATCTGCTCATGACGCTGCGGCTGTGG  
TCCAGCTGA

>343|TRAC\*04 TRAC\_202\_Ensembl\_CDS|TRAC|C-REGION|TR|TRA|None|04

ATGAATGTGTCACAAAGCAAGGATTCTGACGTGCAT  
ATCACAGACAAAACCTGTGCTAGACATGAGGTCTATG  
GACTTTAAGAGCAACGGTGTGCTGGCCTGGAGCAA  
CAAATCCAATTTTGCATGTACAAGCGCCTTCAAGGA  
CAGCGTTATTCCAGCAGACACCTTCTTCCCCGGCA  
CAGAAAGTGTCTGTGATGCCAACCTGGTTGAGAAA  
AGCTTTGAACAGATATGAACCTAAACTTTCAAAAC  
CTGTGAGTGATTGGGTTCCGAATCCTCCTCCTGAAA  
GTGGCCGGGTTAATCTGCTCATGACGCTGCGGCTG  
TGGTCCAGCTGA

>344|TRAC\*05 TRAC\_203\_Ensembl\_CDS|TRAC|C-REGION|TR|TRA|None|05

ACTGGGGTAAACAACCTCTTCTTTGGGACTGGAACA  
AGACTCACCGTTCTTCCAGATCCAGAACCCTGAC  
CCTGCCGTGTACCAGCTGAGAGGCTCTAAATCCAATG  
ACACCTCTGTCTGCCTATTTACTGATTTTGATTCTGTA  
ATGAATGTGTCACAAAGCAAGGATTCTGACGTGCATA  
TCACAGACAAAACCTGTGCTAGACATGAGGTCTATGGA  
CTTTAAGAGCAACGGTGTGCTGGCCTGGAGCAACAA  
ATCCAATTTTGCATGTACAAGCGCCTTCAAGGACAGC  
GTTATTCCAGCAGACACCTTCTTCCCCGGCACAG  
AAAGTGTCTGTGATGCCAACCTGGTTGAGAAAAG  
CTTTGAACAGATATGAACCTAAACTTTCAAAACCT  
GTCAGTGATTGGGTTCCGAATCCTCCTCCTGAAAG  
TGGCCGGGTTAATCTGCTCATGACGCTGCGGCTGT  
GGTCCAGCTGA

>345|TRAC\*06 TRAC\_204\_Ensembl\_CDS|TRAC|C-REGION|TR|TRA|None|06

ATGAATGTGTCACAAAGCAAGGATTCTGACGTGCA  
TATCACAGACAAAACCTGTGCTAGACATGAGGTCTAT

GGACTTTAAGAGCAACGGTGTGCTGGCCTGGAGCAA  
CAAATCCAATTTTGCATGTACAAGCGCCTTCAAGGAC  
AGCGTTATTCCAGCAGACACCTTCTTCCCCGGCACAG  
AAAGTGTCTGTGATGCCAACCTGGTTGAGAAAAGCT  
TTGAAACAGATATGAACCTAAACTTTCAAAACCTGTC  
AGTGATTGGGTTCCGAATCCTCCTCCTGAAAGTGGCC  
GGGTTAATCTGCTCATGACGCTGCGGCTGTGGT  
CCAGCTGA

>346|TRBC1\*01 NW\_001114291|TRBC1|C-REGION|TR|TRB|None|01

AGGACCTGAAAAAGGTGTTCCACCCAAGGTCGCTGT  
GTTTGAGCCATCAGAAGCAGAGATCTCCCACACCCA  
AAAGGCCACGCTGGTGTGCCTGGCCACAGGCTTCTA  
CCCCGACCAGCTGGAGCTGAGCTGGTGGGTGAAACGG  
GAAAGAGGTGCACAGTGGGTCAGCAGGACCCCA  
GCCCCCAAGGAGCAGCCCGCCCTCGAGGACTCCAG  
ATACTGCCTGAGCAGCCGCTGAGGGTCTCGGCCAC  
CTTCTGGCACAACCCCGCAACCACTTCGCTGCCAA  
GTCCAGTTCTATGGGCTCTCGGAGGATGACGAGTGGA  
CCGAGGACAGGGACAAGCCCATCACCCAAAAGATCAG  
CGCCGAGGCTGGGGTAGAGCAGACTGTGGCTTCACC  
TCGGTGTCTACCAGCAAGGGTCTGTCTGCCACCAT  
CCTCTATGAGATCCTGCTGGGGAAGGCCACCCTGTATG  
CTGTGCTGGTCAGTGCCCTCATGTTGATGGCCAT  
GGTCAGAGGAAGGATTC

>347|TRBC1\*02 IMGT000073|TRBC1|C-REGION|TR|TRB|None|02

AGGACCTGAAAAAGGTGTTCCACCCAAGGTCGCTGTG  
TTTGAGCCATCAGAAGCAGAGATCTCCCACACC  
CAAAAGGCCACGCTGGTGTGCCTGGCCACAGGCTT  
CTACCCCGACCAGCTGGAGCTGAGCTGGTGGGTGAA  
CGGAAAAGAGGTGCACAGTGGGGTCAGCACGGACCC  
ACAGCCCCTCAAGGAGCAGCCCGCCCTCGAGGACTCCA  
GATACTGCCTGAGCAGCCGCTGAGGGTCTCAGCCACC  
TTCTGGCACAACCCCGCAACCACTTCGCTGCCAAGT  
CCAGTTCTATGGGCTCTCGGAGGATGACGAGTG  
GACCAGGACAGGGACAAGCCCATCACCCAAA  
AGATCAGCGCCGAGGTCTGGGGTAGAGCAGA  
CTGTGGCTTCACTCAGTGTCTACCAGCAA  
GGGGTCTGTCTGCCACCATCCTCTATGAGATC  
CTGCTGGGGAAGGCCTCCCTGTATGCTGTGCT  
GGTCAGTGCCCTCATGTTGATGGCCATGGTCA  
AGAGGAAGGATTC

>348|TRBC2\*03 IMGT000073|TRBC2|C-REGION|TR|TRB|None|01

AGGACCTGAAAAAGGTGTTCCACCCAAGGTCGC  
TGTGTTTGAGCCATCAGAAGCAGAGATCTCCCAC  
ACCCAAAAGGCCACGCTGGTGTGCCTGGCCACAG  
CTTCTACCCCGACCAGCTGGAGTTGAGCTGGTGGG  
TGAACGGGAAAGAGGTGCACAGTGGGGTCAGCACG  
GACCCACAGCCCCTCAAGGAGCAGCCACCCTCGA  
GGACTCCAGATACTGCCTGAGCAGCCGCTGAGGG  
TCTCGGCCACCTTCTGGCACAACCCCGCAACCACT  
TCCGCTGCCAAGTCCAGTTCTATGGGCTCTCGGAGGA

TGACGAGTGGACCGAGGACAGGGACAAGCCCATCAC  
 CCAAAGATCAGCGCTGAGGCCTGGGGTAGAGCAG  
 ACTGTGGCTTACCTCTGAGTCTTACCAGCAAGGGG  
 TCCTGTCTGCCACCATCCTCTATGAGATCTTGCTAGG  
 GAAGGCCACCTTGATGCCGTGCTGGTCAGTGCCCTC  
 GTGCTGATGGCCATGGTCAAGAGAAAGGATTCC

This resulted in an initial set of 348 sequences. We then checked these sequences for premature stop codons, frameshifts, and other potential problems using 10x's enclone software, v0.5.42. This identified 44 problematic sequences which were removed, leaving us with a final total of 304 VDJ segments.

## GEX Alignment and TCR Reconstruction

Samples were aligned using the Cellranger multi pipeline (v6.0.2), with VDJ libraries listed as "vdj-t" to indicate T cell libraries. Samples were aggregated with the Cellranger aggr pipeline (v6.0.2) with `normalize=none`. Our reference transcriptome was created with the Cellranger makeref command, and used genome assembly Mmul\_10 as the reference genome (37), and Ensembl v104 as the reference set of annotations.

## GEX Filtering and QC

We used FASTQC to assess the quality of our sequencing data. After alignment of this data, we loaded the `filtered_feature_bc_matrix.h5` file from Cellranger multi into Seurat and removed genes which were present in less than 5 cells. This resulted in a dataset with 38,147 cells by 16,163 genes. Following the recommendations in Lucken and Theis (38), we analyzed the total transcripts detected and total genes detected for each sample to determine appropriate thresholds and retained cells with 500 to 6,000 genes detected and 1,800 to 40,000 transcripts detected, and less than 5% of aligned reads originating from the mtDNA. We then applied SCTransform (39) to normalize the data, reduced the dimensionality of the dataset using PCA (retained 22 PC's after check of ElbowPlot), clustered the data using Seurat's FindClusters function with a resolution of 0.2, and subsetted the dataset to T cells by removing two clusters that were not enriched for the T cell genes CD3E, CD4, CD8A, or TRAC. This resulted in a dataset with 28,646 cells by 15,904 genes. We then repeated the above procedure from SCTransform to clustering using 23 PC's.

We then limited the dataset to samples from the PBMC, the MLR experiments, and the GVHD target organs. We then removed genes present in less than 5 cells, resulting in a dataset with 23,618 cells by 15,195 genes. This dataset was normalized using the same pipeline previously described in this section, retaining 22 PC's from the PCA.

## Identification of Clonotypes

Clonotypes used in the gene expression analysis were identified using cellranger's default settings in "cellranger vdj" for the scTCR-Seq libraries. Clonotypes used for the Shannon Diversity metric calculations (Figure 2C) were based on grouping cells by the nucleotide sequence of the CDR3 region of the alpha chain, which was identified for 80% to 99% of the cells in each of the 12 samples.

As discussed in the Results section, the clonotypes used for the alpha chain and beta chain Morisita heatmaps (Figure 2, panels E, F) were identified by grouping together T cells on the basis of the CDR3 region in the alpha chain or beta chain. This is to provide a more stringent test of the specificity of clonotype calling, as Cellranger's default settings do not allow for clonotypes to be shared across different donors. The Morisita index was calculated using the "vegan" package in R.

## Differential Expression (DE) Tests

DE tests were carried out as Wilcoxon Rank Sum tests in Seurat, using the default settings. Results with an adjusted p value <0.05 were considered significant.

## Scoring of Cells With Gene Signatures Using VISION

We used VISION to apply gene signatures to the normalized expression data for the analyzed T cells. We used the C7 collection of immunological signatures from MSigDB, and ten signatures from the C2 curated collection that contained the key phrases "allo" or "graft" to identify potential alloreactivity signatures. To test for differences in signature enrichment between cells belonging to MLR+ and MLR- clonotypes within an organ, we used the Wilcoxon test.

## RESULTS

### Efficient Amplification of RM TCR Alpha and Beta Chains

Immunological studies in RM have been performed for decades, and have significantly advanced our understanding of adaptive T cell immunity in health and disease. However, in-depth characterization of RM T cell clonality and associated T cell function on a single cell level have been hindered by a paucity of available methods, particularly the ability to efficiently amplify and reconstruct the RM alpha and beta TCR chains. Here we present a robust platform for RM TCR amplification leveraging the well-established human 5' 10x Genomics single cell sequencing platform. To accomplish this, we optimized primer pairs adapted to utilize a nested PCR approach analogous to that of the 10x human and mouse workflows, thereby maximizing the specificity of amplification, with primer sets targeting the constant regions of the RM alpha and beta chains ('TRAC' and 'TRBC', respectively). The primers targeting the beta chain were specifically designed to amplify both TRBC1 and TRBC2. Primer length, CG content and annealing temperatures were adjusted to be used with the forward primers supplied in the human 5' 10x Genomics kit. Cycling conditions were modified from the original 10x protocol to allow optimal amplification of the targeted region in RM (Tables 1, 2). We have named this new resource 'RM-scTCR-Seq'.

RM-scTCR-Seq primers annealed to the alpha and beta RM constant region and amplified transcripts covering the complete alpha and beta loci including the variable V and J regions for the alpha as well as V, D and J regions for the beta locus.

(**Figure 1A**). Our assembled contigs extend past the V region, which likely represents unannotated UTR sequences. Such UTR sequences are annotated in the human and mouse VDJ references (40) and can be seen in the assembled contigs for 10x Genomics’ human and mouse sample datasets.

We assessed the quality of our primers using summary statistics from 10x’s ‘Cellranger’ software (a pipeline for alignment, quantification, and evaluation of 10x Genomics-generated single-cell libraries), and found that our primers

consistently amplify high-quality reads from the TCR alpha and beta chains. For this assessment, we prepared peripheral blood mononuclear cells (PBMCs) from three representative RMs (animal IDs: R.276, R.279, R.319) and used these PBMCs to perform RM-scTCR-Seq. We observed that 49-52% of the aligned reads mapped to the alpha chain and 22-25% of the reads aligned to the beta chain (**Figure 1Bi**, ii and **Table S2**) in the three RMs, with  $\geq 73\%$  of total reads mapping to any V(D)J gene (including to gamma and delta chain sequences).

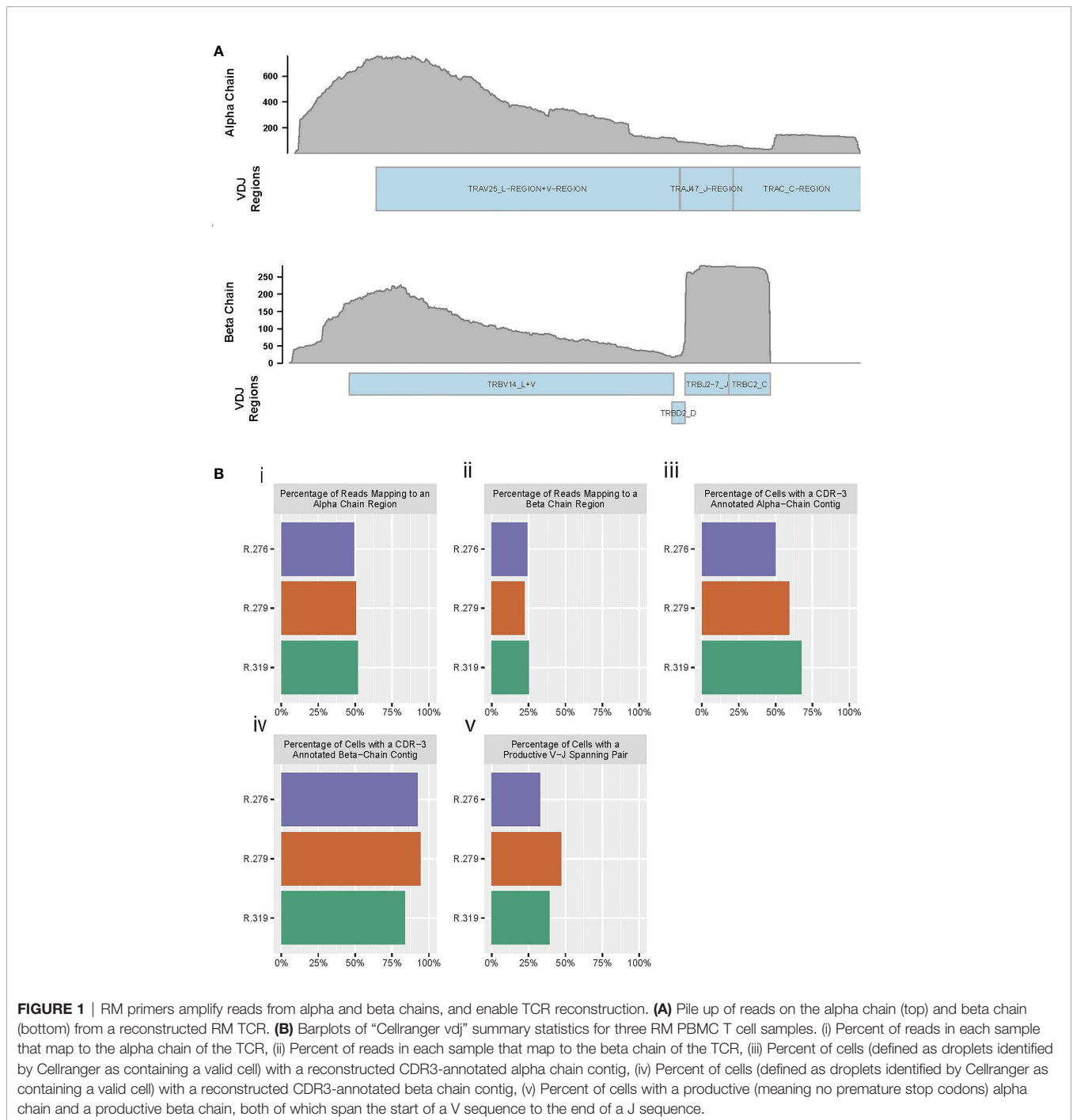


**FIGURE 1** | RM primers amplify reads from alpha and beta chains, and enable TCR reconstruction. (**A**) Pile up of reads on the alpha chain (top) and beta chain (bottom) from a reconstructed RM TCR. (**B**) Barplots of “Cellranger vdj” summary statistics for three RM PBMC T cell samples. (i) Percent of reads in each sample that map to the alpha chain of the TCR, (ii) Percent of reads in each sample that map to the beta chain of the TCR, (iii) Percent of cells (defined as droplets identified by Cellranger as containing a valid cell) with a reconstructed CDR3-annotated alpha chain contig, (iv) Percent of cells (defined as droplets identified by Cellranger as containing a valid cell) with a reconstructed CDR3-annotated beta chain contig, (v) Percent of cells with a productive (meaning no premature stop codons) alpha chain and a productive beta chain, both of which span the start of a V sequence to the end of a J sequence.

In addition to demonstrating that the sequencing reads mapped to known TCR loci, we were also able to reconstruct the alpha and beta chains from these reads (**Figure 1Biii**, iv and **Table S2**). The Complementarity-determining region (CDR) 3 is the most variable of the CDR regions, and spans the V and J regions; thus, identification of this sequence is useful as a benchmark for reconstruction quality (41). As such, an ideal reconstruction of the alpha chain or beta chain would completely span the V-to-J region, and enable inference of the CDR3 sequence (42, 43). Using the preceding criteria as our standard for a high-quality alpha or beta TCR chain reconstruction, we observed that 50 to 67% of the 10X droplets identified as cells by Cellranger produced a full length, CDR3-annotated alpha chain (**Figure 1Biii** and **Table S2**). Inspecting the beta chain, we found that a high-quality beta chain could be constructed for 83% to 94% for these same cells (**Figure 1Biv** and **Table S2**). Full reconstruction of the TCR requires both an alpha chain and a beta chain that span the V and J regions, and ideally are productive (no premature stop codons). We identified both alpha and beta chains in 32 to 47% of cells examined (**Figure 1Bv** and **Table S2**).

These data demonstrate, for the first time, efficient amplification of the RM TCR alpha and beta region by utilizing optimized RM primer pairs compatible with the human 5' 10x Genomics single cell sequencing platform. Amplified reads enabled high quality beta chain reconstruction in almost all, and reconstruction of full TCRs (alpha and beta chains) in a significant number of sequenced cells.

## RM-scTCR Seq Enables Tracking of T Cell Clonotypes in Allogenic Mixed Lymphocyte Reactions

Identification of T cell clonotypes using *in vitro* assays or *in vivo* disease models enables the evaluation of the clonal repertoire, clonal dynamics, and the tracking of specific T cells over time. To validate our single cell TCR sequencing and analysis pipeline, we first utilized an *in vitro* allo-proliferation assay: the mixed lymphocyte reaction (MLR) (44–47). To perform these studies, PBMCs from 4 RM were irradiated with 3500 cGy and used to stimulate “responder” PBMCs from MHC-disparate RM. The responder PBMCs were labeled with cell trace violet (CTV), a cell dye which dilutes with proliferation. After five days of allo-stimulation, responder T cell were sorted into three populations: CTV High (non-proliferating T cells), CTV Mid (intermediate proliferation, 3–5 cell divisions) and CTV Low (highly proliferating T cells, demonstrating > 7 cell divisions by flow cytometry), (**Figures 2A, B**). We applied the RM-scTCR-Seq pipeline to analyze TCR diversity, measured by the nucleotide sequence of the CDR3 alpha chain, in each of these fractions, and assessed this diversity using the Shannon index (48) (**Table S2**). As demonstrated in **Figure 2C**, the highest proliferating population displayed the lowest Shannon diversity (CTV Low Shannon index = 7.52 – 8.40), indicating highest clonality, while diversity increased with the less proliferating cells (CTV Mid Shannon index = 7.61 – 8.93 and CTV High Shannon index = 7.94 – 9.09). The difference in the Shannon index comparing the CTV High vs

CTV low samples, after applying the Hutcheson t-test was significant with a p-value of < 0.01 for all four samples tested (49).

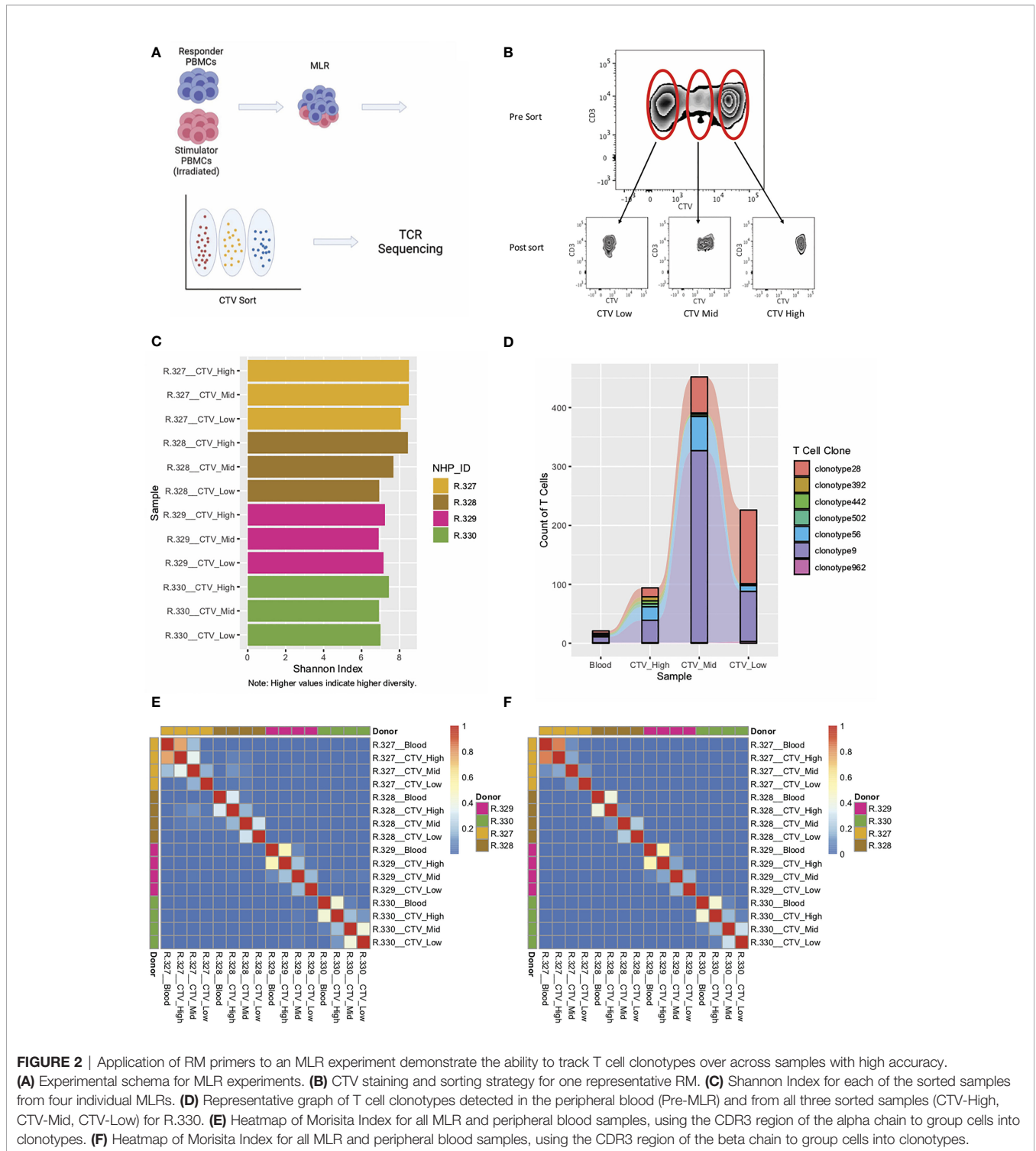
Using the RM-scTCR-Seq pipeline, we were also able to track individual clonotypes throughout the three MLR peaks (**Figure 2D**) using either their alpha or their beta chain clonotype. While we are able to identify individual clones and track clonal changes over time, it should be noted that the 10X platform is limited in its ability to measure large-scale T cell population-based clonal expansion and deletion, given that 10X is designed to analyze ~10,000 cells. Bulk RM TCR Seq, which has the capacity to measure millions of input cells, will be more suitable to answer these population-based questions. A RM-specific platform for bulk TCRseq is currently under development by our research group.

To further assess our ability to accurately track T cell clonotypes *in vitro*, and to quantify TCR similarities/differences between T cells isolated from different animals, we calculated the Morisita Index (‘MI’, measuring the similarity of two repertoires, or, the reproducibility of a single repertoire between different samples) (48, 50) between all pairs of samples from the MLR experiment. We analyzed these data using the CDR3 regions of the alpha chain (**Figure 2E**) and the beta chain (**Figure 2F**).

As has been previously demonstrated, the vast majority of TCR clonotypes in our assay were private to the individual animal, with low levels of similarity when comparing TCR clonotypes between different animals (MI < 0.08, indicating minimal overlap in the TCR repertoire, **Figures 2E, F**). As expected, the highest level of similarity was observed between responder PBMCs in the ‘Blood’ sample (T cells isolated from peripheral blood pre MLR) and T cells in the non-proliferating population (‘CTV high’). Importantly we were also able to identify clonotypes that existed in both the Blood sample and the high-proliferating population (**Figures 2E, F**), substantiating the ability of RM-scTCR-Seq to track clonotypes as they proliferated *in vitro*. The low Morisita indices for comparison of samples between different donors, using either alpha chain MI (MI < 0.08) or beta chain MI (MI < 0.001), demonstrate the specificity of the RM-scTCR-Seq approach (**Figures 2E, F**) and validate that clonotype tracking can be performed by utilizing the TCR alpha or beta chains.

## In Vitro Predicted Alloreactive T Cell Clonotypes Exhibit an In Vivo aGVHD Expression Program in the Spleen and Liver

We next performed *in vivo* clonotype tracking in HCT recipients who developed aGVHD, in order to trace specific TCRs previously identified as allo-proliferating in an *in vitro* MLR. To accomplish this, we first performed MLR assays using donor and recipient PBMCs from transplants in which recipients subsequently developed severe aGVHD (28). For these assays, responder PBMCs were from donor animals R.276, R.279, R.319, and stimulator PBMCs were from recipient animals R.227, R.276 and R.312, respectively (28). Terminal analysis of spleen and liver infiltrating donor T cells was performed 8 days after HCT, during active aGVHD (28). Sorted T cells were analyzed with



5’scrNA-Seq using the 10X platform, and clonotype-tracking was performed using the RM-scTCR-Seq pipeline. The number of cells sequenced and the number of cells with unique alpha and beta TCR chains are found in **Table S2**.

We first assessed our ability to track clonotypes across samples by applying the MI to all of the scTCR-Seq libraries (**Figure 3A**). As

expected, in all three animals, measurable TCR clonal overlap could be detected in T cells sorted from recipient liver and spleen, consistent with infiltration of activated T cell clonotypes into both of these organs. Overlap of alloreactive (highly proliferating) clonotypes from the MLR with clonotypes derived from both the spleen and the liver was also evident (**Figure 3A**). Next, we

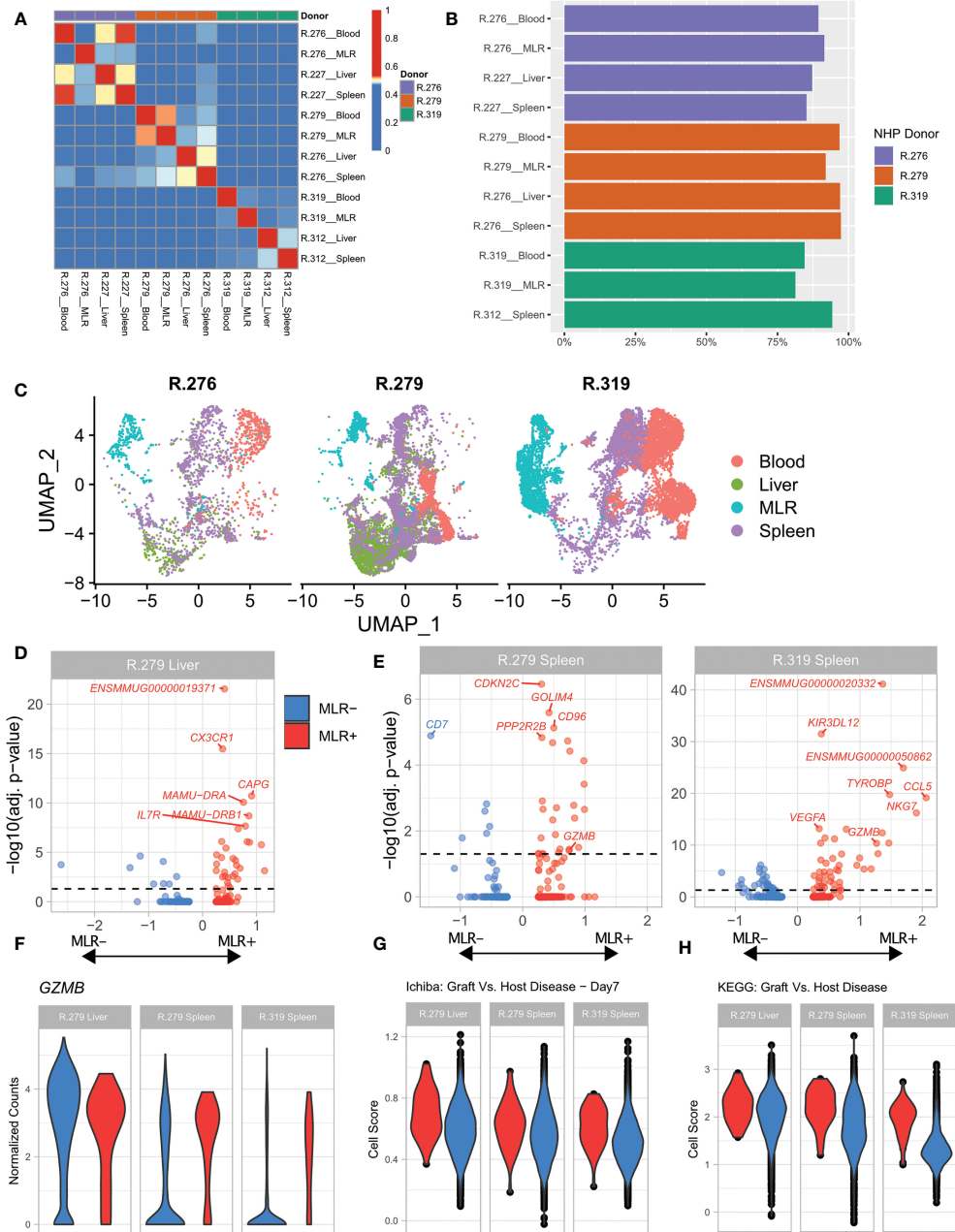


**FIGURE 3** | Allo-proliferative T cell clonotypes identified in an MLR exhibit aGVHD-specific gene expression programs in the spleen and the liver. **(A)** Heatmap of the Morisita Index for all analyzed samples. **(B)** Percentage of cells assigned to a specific T cell clonotype using RM-scTCR-Seq that also had high-quality gene expression data using the 10X gene expression platform. **(C)** UMAP of cells from each donor NHP, colored by sample type. Blood = T cells sorted from the blood. MLR= T cells subjected to a MLR. Spleen = T cells purified from the spleen during severe aGVHD. Liver = T cells purified from the liver during severe aGVHD. **(D)** Volcano plots of differential expression between MLR+ and MLR- detected clonotypes within one liver sample. **(E)** Volcano plots of differential expression between MLR+ and MLR- detected clonotypes within two spleen samples. **(F)** Violin plot of *GZMB* expression between MLR+ (red) and MLR- (blue) cells within two spleen samples (from R.279 and R.319) and one liver sample (from R.279). **(G)** Violin plot of T cells scored with the Ichiba Graft Versus Host Disease signature (35), colored by the detection of a clonotype in MLR+ (red) or MLR- (blue) samples.  $P < 0.05$  for the comparisons in the liver, and both spleen samples. **(H)** Violin plot of T cells scored with the KEGG Graft Versus Host Disease signature (51) colored by the detection of a clonotype in MLR+ (red) or MLR- (blue) samples.  $P < 0.001$  for the comparisons in the liver, and both spleen samples.

confirmed that the majority of cells with trackable TCRs by RM-scTCR-Seq cells also had a corresponding barcode in the scRNA-Seq GEX library after quality control and filtering. We found that at least 75% of the cells with a valid scTCR-Seq library (assessed by Cell Ranger) in each sample also had a valid corresponding scRNA-Seq barcode (**Figure 3B**) confirming the efficiency of the assay. After alignment, filtering based on quality metrics, and dimensionality reduction, we plotted a UMAP of the analyzed cells ( $n = 23,618$  total cells analyzed from three RM) separated according to each transplant recipient (**Figure 3C** and **Table S2** - GEX Cell Count After Filtering).

We then characterized cells isolated from the spleen and liver by whether they could be matched with an alloproliferating MLR clonotype (termed 'MLR+') or not (termed 'MLR-'). Each MLR+ cluster incorporated at least 37 cells (**Table 3**). Using these definitions of MLR+ and MLR-, we conducted a gene expression test of MLR+ versus MLR- T cells within two spleen samples and one liver sample with large numbers of MLR clonotypes, to identify differentially expressed (DE) genes. The volcano plots in **Figures 3D, E** demonstrate these DE genes, and highlight the top 5 annotated genes in each comparison (top genes with only an Ensembl ID are also identified). This analysis identified several known markers of alloreactivity in each sample. *GZMB*, a well-recognized aGVHD-associated gene (28, 52) was identified as a DE gene in both spleen samples (**Table S3**). We further interrogated the expression of *GZMB* at the level of each individual cell, to understand its variability within the MLR+ and MLR- populations. As expected, a violin plot of *GZMB* (**Figure 3F**) demonstrated that the spleen MLR+ samples had higher, less variable expression of *GZMB* compared to the spleen MLR- samples, which demonstrated a wider distribution of expression, with a larger proportion of low-expressing cells. To further evaluate gene expression in the MLR+ and MLR- cells, we used VISION (53) to score each cell using a set of previously curated immunological and alloreactivity signatures. As shown in **Figures 3G, H**, MLR+ cells from the liver and spleen enriched for the Ichiba: Graft versus Host Disease gene signature compared to MLR- cells (**Figure 3G**,  $p < 0.05$ ) (35) as well as for the KEGG Graft versus host disease signature (**Figure 3H**,  $p < 0.01$ ) (51).

These results demonstrate the feasibility of combining RM-scTCR-Seq and scRNA-Seq to identify and interrogate alloreactive T cell clonotypes in aGVHD target organs in RM, providing proof-of-concept of the *in vivo* utility of the RM-scTCR-Seq pipeline.

## DISCUSSION

TCR repertoire analysis has become a fundamental tool to understand the immune responses to infections and vaccines, as well as the immunopathogenesis of rejection after solid organ transplantation, and GVHD after HCT (2, 46, 47, 54–58). In murine and human studies, the introduction of VDJ target enrichment combined with single cell sequencing platforms has enabled the interrogation of transcriptional profiling of single T cells at an unprecedented level of accuracy (42, 43). However, paired single cell T cell receptor and transcriptional studies in RM have been impeded by the lack of a validated platform to amplify and reconstruct alpha and beta TCR sequences (59–61). This study demonstrates successful identification and tracking of RM single T cell clonotypes by utilizing customized primers compatible with the human 5' 10x Genomics single cell sequencing platform, and by significantly improving alignment of RM sequencing results by creating a custom reference for the RM TCR alpha and beta chains.

Prior to the work described herein, two major limitations significantly hindered the development of T cell clonotype tracking in RM. They were (1): The lack of optimized, single cell sequencing-compatible primers covering both the TCR alpha and beta region for RM; (2) The poor genomic annotation of the alpha and beta loci in RM, which resulted in inadequate reconstruction of amplified VDJ PCR reads. To address both of these technical barriers, we have designed a robust set of RM-specific TCR primer pairs which anneal to the constant region of the alpha and beta TCR loci, and which are compatible with the commonly used single cell sequencing platform from 10x Genomics. Optimizing PCR cycling and temperature conditions resulted in efficient amplification of the alpha and beta regions of the RM TCR and generated productive TCR reconstructions. Additionally, we created an updated reference for the TCR alpha and beta chain region, enhancing our ability to annotate the assembled RM TCR's.

We demonstrated amplification of highly specific TCR regions with >73% of total reads mapping to any V(D)J gene. We note that this mapping efficiency is somewhat less than the ~91% of reads mapping to the human VDJ reference, in a human dataset provided by 10x ([www.10xgenomics.com/resources/dataset](http://www.10xgenomics.com/resources/dataset)). The difference in the alignment rate may be explained by differing levels of annotation for these organisms: 10x provides human references which have been refined over time, but this resource does not exist for RM, which necessitated our creation of a new reference (see *Methods*) by combining elements of the Ensembl and IMGT references, and then carefully filtering out sequences identified by 10x's enclone software that contained errors (such as premature stop codons, see *Methods*). As annotation of the RM TCR improves, we anticipate some gains in read mapping. As mentioned earlier, we have noticed that UTR regions are annotated in the human and mouse VDJ references, and we expect that addition of these sequences to the RM reference will improve alignment rates. We additionally tested whether our reads adequately covered all genomic V(D)J regions and confirmed that in the 30 primary VDJ samples analyzed, reads mapped to 91% (179 of 196) of all V(D)J regions from our reference (**Table S5**). Additionally, **Figure S1** provides

**TABLE 3** | Sample sizes for MLR+ and MLR- cells in GEX data.

NHP	Organ	MLR Status	Cell Count
R.279	Liver	MLR-	4,025
R.279	Liver	MLR+	58
R.279	Spleen	MLR-	2,773
R.279	Spleen	MLR+	37
R.319	Spleen	MLR-	4,632
R.319	Spleen	MLR+	39

detailed information regarding alpha-chain, beta-chain, and CDR3 region length, which were all with the expected length range, further supporting the robustness of this method.

Sufficient alignment was also demonstrated by the ability of the RM-scTCR-Seq pipeline to detect allo-proliferating clonotypes using an *in vivo* RM model of aGVHD. While bulk TCR-Seq is well-suited for providing a comprehensive profile of the diversity of T cell clonotypes in a given sample due to its ability to profile large numbers of cells (59, 61), scTCR-Seq is unique in its ability to be paired with other single-cell technologies, allowing users to tag each T cell with its clonal identity, and measure each cell's gene expression profile as performed here (9). These clonotypes can also be interrogated for their protein expression or epigenetic profiles, or other features of interest (62, 63). Most importantly, these individual clonotypes can be tracked *in vivo*, to better map the clonal architecture of protective versus pathogenic T cell responses, in target tissues that are far more accessible in NHP than in patient samples. In this study utilizing RM-scTCR-Seq, we were able to detect allo-proliferative clonotypes in *in vitro* MLR experiments and track their *in vivo* alloreactive and cytotoxic potential by transcriptional analysis of tissue-infiltrating T cells. We expect that future RM-scTCR-Seq studies from GVHD target tissues including the GI tract and skin will provide further insights into mechanisms controlling T cell alloreactivity, and enhance our ability to identify GVHD-specific targetable pathways.

Given the central importance of NHP models to our understanding of protective and pathogenic immunity, and to the development of novel immune-based therapeutics, the application of RM-scTCR-Seq is expected to have wide application, and further advance the ability of NHP to model human disease.

## DATA AVAILABILITY STATEMENT

The original contributions presented in the study are publicly available. This data can be found here: <https://www.ncbi.nlm.nih.gov/geo/query/acc.cgi?acc=GSE190268>.

## REFERENCES

- Arstila TP, Casrouge A, Baron V, Even J, Kanellopoulos J, Kourilsky P. A Direct Estimate of the Human Alphabeta T Cell Receptor Diversity. *Science* (1999) 286(5441):958–61. doi: 10.1126/science.286.5441.958
- Suessmuth Y, Mukherjee R, Watkins B, Koura DT, Finstermeier K, Desmarais C, et al. CMV Reactivation Drives Posttransplant T-Cell Reconstitution and Results in Defects in the Underlying TCRbeta Repertoire. *Blood* (2015) 125(25):3835–50. doi: 10.1182/blood-2015-03-631853
- Li B, Li T, Pignon JC, Wang B, Wang J, Shukla SA, et al. Landscape of Tumor-Infiltrating T Cell Repertoire of Human Cancers. *Nat Genet* (2016) 48(7):725–32. doi: 10.1038/ng.3581
- Dziubianau M, Hecht J, Kuchenbecker L, Sattler A, Stervbo U, Rodelsperger C, et al. TCR Repertoire Analysis by Next Generation Sequencing Allows Complex Differential Diagnosis of T Cell-Related Pathology. *Am J Transplant* (2013) 13(11):2842–54. doi: 10.1111/ajt.12431
- Pogorelyy MV, Minervina AA, Touzel MP, Sycheva AL, Komech EA, Kovalenko EI, et al. Precise Tracking of Vaccine-Responding T Cell Clones Reveals Convergent and Personalized Response in Identical Twins. *Proc Natl Acad Sci USA* (2018) 115(50):12704–9. doi: 10.1073/pnas.1809642115

## ETHICS STATEMENT

The animal study was reviewed and approved by Massachusetts General Hospital Animal Care and Use Committee and Biomere Animal Care and Use Committee.

## AUTHOR CONTRIBUTIONS

Conceptualization: UG, RAF, VT, and LK. Methodology: UG, RAF, JK, VT, and CM. Investigation: RAF, UG, JK, XR, LC, JFL, and CM. Visualization: JK and UG. Supervision: LK, AS, PK, and LC. Writing—original draft: UG, JK, and LK. Writing—review & editing: UG, JK, RAF, XR, JFL, PK, LC, VT, AKS, and LK. All authors contributed to the article and approved the submitted version.

## FUNDING

UG is supported by the Helen Gurley Brown Foundation and the National Cancer Center. JK is supported by the NIH (5T32HL007574-40) and the National Cancer Center. VT is supported by an ASTCT New Investigator Award and the CIBMTR/Be The Match Foundation Amy Strelzer Manasevit Research Program Award. AS is supported by the Searle Scholars Program, the Beckman Young Investigator Program, a Sloan Fellowship in Chemistry, and the NIH (5U24AI118672, 2R01HL095791). LK is supported by NIH grants U19 AI1051731, R01 HL095791, P01 HL158504, and by a Leukemia and Lymphoma Society TRP grant.

## SUPPLEMENTARY MATERIAL

The Supplementary Material for this article can be found online at: <https://www.frontiersin.org/articles/10.3389/fimmu.2021.804932/full#supplementary-material>

- Freeman JD, Warren RL, Webb JR, Nelson BH, Holt RA. Profiling the T-Cell Receptor Beta-Chain Repertoire by Massively Parallel Sequencing. *Genome Res* (2009) 19(10):1817–24. doi: 10.1101/gr.092924.109
- Robins HS, Campregher PV, Srivastava SK, Wachter A, Turtle CJ, Kahsai O, et al. Comprehensive Assessment of T-Cell Receptor Beta-Chain Diversity in Alphabeta T Cells. *Blood* (2009) 114(19):4099–107. doi: 10.1182/blood-2009-04-217604
- Carter JA, Preall JB, Grigaityte K, Goldfless SJ, Jeffery E, Briggs AW, et al. Single T Cell Sequencing Demonstrates the Functional Role of Alphabeta TCR Pairing in Cell Lineage and Antigen Specificity. *Front Immunol* (2019) 10:1516. doi: 10.3389/fimmu.2019.01516
- Stubbington MJT, Lonnberg T, Proserpio V, Clare S, Speak AO, Dougan G, et al. T Cell Fate and Clonality Inference From Single-Cell Transcriptomes. *Nat Methods* (2016) 13(4):329–32. doi: 10.1038/nmeth.3800
- Buggert M, Vella LA, Nguyen S, Wu VH, Chen Z, Sekine T, et al. The Identity of Human Tissue-Emigrant CD8(+) T Cells. *Cell* (2020) 183(7):1946–61.e15. doi: 10.1016/j.cell.2020.11.019
- Merkenschlager J, Finkin S, Ramos V, Kraft J, Cipolla M, Nowosad CR, et al. Dynamic Regulation of TFH Selection During the Germinal Centre Reaction. *Nature* (2021) 591(7850):458–63. doi: 10.1038/s41586-021-03187-x

12. Messaoudi I, Estep R, Robinson B, Wong SW. Nonhuman Primate Models of Human Immunology. *Antioxid Redox Signal* (2011) 14(2):261–73. doi: 10.1089/ars.2010.3241
13. Ziegler CGK, Allon SJ, Nyquist SK, Mbano IM, Miao VN, Tzouanas CN, et al. SARS-CoV-2 Receptor ACE2 Is an Interferon-Stimulated Gene in Human Airway Epithelial Cells and Is Detected in Specific Cell Subsets Across Tissues. *Cell* (2020) 181(5):1016–35 e19. doi: 10.1016/j.cell.2020.04.035
14. Corbett KS, Edwards DK, Leist SR, Abiona OM, Boyoglu-Barnum S, Gillespie RA, et al. SARS-CoV-2 mRNA Vaccine Design Enabled by Prototype Pathogen Preparedness. *Nature* (2020) 586(7830):567–71. doi: 10.1038/s41586-020-2622-0
15. Mercado NB, Zahn R, Wegmann F, Loos C, Chandrashekar A, Yu J, et al. Single-Shot Ad26 Vaccine Protects Against SARS-CoV-2 in Rhesus Macaques. *Nature* (2020) 586(7830):583–8. doi: 10.1038/s41586-020-2607-z
16. Corbett KS, Flynn B, Foulds KE, Francica JR, Boyoglu-Barnum S, Werner AP, et al. Evaluation of the mRNA-1273 Vaccine Against SARS-CoV-2 in Nonhuman Primates. *N Engl J Med* (2020) 383(16):1544–55. doi: 10.1056/NEJMoa2024671
17. McMahan K, Yu J, Mercado NB, Loos C, Tostanoski LH, Chandrashekar A, et al. Correlates of Protection Against SARS-CoV-2 in Rhesus Macaques. *Nature* (2021) 590(7847):630–4. doi: 10.1038/s41586-020-03041-6
18. Colonna L, Peterson CW, Schell JB, Carlson JM, Tkachev V, Brown M, et al. Evidence for Persistence of the SHIV Reservoir Early After MHC Haploidentical Hematopoietic Stem Cell Transplantation. *Nat Commun* (2018) 9(1):4438. doi: 10.1038/s41467-018-06736-7
19. Chen Z. Monkey Models and HIV Vaccine Research. *Adv Exp Med Biol* (2018) 1075:97–124. doi: 10.1007/978-981-13-0484-2\_5
20. Barouch DH, Alter G, Broge T, Linde C, Ackerman ME, Brown EP, et al. Protective Efficacy of Adenovirus/Protein Vaccines Against SIV Challenges in Rhesus Monkeys. *Science* (2015) 349(6245):320–4. doi: 10.1126/science.aab3886
21. Fitch Z, Schmitz R, Kwun J, Hering B, Madsen J, Knechtle SJ. Transplant Research in Nonhuman Primates to Evaluate Clinically Relevant Immune Strategies in Organ Transplantation. *Transplant Rev (Orlando)* (2019) 33(3):115–29. doi: 10.1016/j.trre.2019.03.002
22. Knechtle SJ, Shaw JM, Hering BJ, Kraemer K, Madsen JC. Translational Impact of NIH-Funded Nonhuman Primate Research in Transplantation. *Sci Transl Med* (2019) 11(500). doi: 10.1126/scitranslmed.aau0143
23. Miller WP, Srinivasan S, Panoskaltis-Mortari A, Singh K, Sen S, Hamby K, et al. GVHD After Haploidentical Transplantation: A Novel, MHC-Defined Rhesus Macaque Model Identifies CD28<sup>+</sup> CD8<sup>+</sup> T Cells as a Reservoir of Breakthrough T-Cell Proliferation During Costimulation Blockade and Sirolimus-Based Immunosuppression. *Blood* (2010) 116(24):5403–18. doi: 10.1182/blood-2010-06-289272
24. Furlan SN, Watkins B, Tkachev V, Flynn R, Cooley S, Ramakrishnan S, et al. Transcriptome Analysis of GVHD Reveals Aurora Kinase A as a Targetable Pathway for Disease Prevention. *Sci Transl Med* (2015) 7(315):315ra191. doi: 10.1126/scitranslmed.aad3231
25. Furlan SN, Watkins B, Tkachev V, Cooley S, Panoskaltis-Mortari A, Betz K, et al. Systems Analysis Uncover Inflammatory Th/Tc17-Driven Modules During Acute GVHD in Monkey and Human T Cells. *Blood* (2016) 128(21):2568–79. doi: 10.1182/blood-2016-07-726547
26. Watkins BK, Tkachev V, Furlan SN, Hunt DJ, Betz K, Yu A, et al. CD28 Blockade Controls T Cell Activation to Prevent Graft-Versus-Host Disease in Primates. *J Clin Invest* (2018) 128(9):3991–4007. doi: 10.1172/JCI98793
27. Uchida N, Nassehi T, Drysdale CM, Gamer J, Yapundich M, Bonifacino AC, et al. Busulfan Combined With Immunosuppression Allows Efficient Engraftment of Gene-Modified Cells in a Rhesus Macaque Model. *Mol Ther* (2019) 27(9):1586–96. doi: 10.1016/j.yth.2019.05.022
28. Tkachev V, Kaminski J, Potter EL, Furlan SN, Yu A, Hunt DJ, et al. Spatiotemporal Single-Cell Profiling Reveals That Invasive and Tissue-Resident Memory Donor CD8<sup>+</sup> T Cells Drive Gastrointestinal Acute Graft-Versus-Host Disease. *Sci Transl Med* (2021) 13(576). doi: 10.1126/scitranslmed.abc0227
29. Burwitz BJ, Wu HL, Abdulhaqq S, Shriver-Munsch C, Swanson T, Legasse AW, et al. Allogeneic Stem Cell Transplantation in Fully MHC-Matched Mauritian Cynomolgus Macaques Recapitulates Diverse Human Clinical Outcomes. *Nat Commun* (2017) 8(1):1418. doi: 10.1038/s41467-017-01631-z
30. Page A, Srinivasan S, Singh K, Russell M, Hamby K, Deane T, et al. CD40 Blockade Combines With CTLA4Ig and Sirolimus to Produce Mixed Chimerism in an MHC-Defined Rhesus Macaque Transplant Model. *Am J Transplant* (2012) 12(1):115–25. doi: 10.1111/j.1600-6143.2011.03737.x
31. Tkachev V, Furlan SN, Watkins B, Hunt DJ, Zheng HB, Panoskaltis-Mortari A, et al. Combined OX40L and mTOR Blockade Controls Effector T Cell Activation While Preserving Treg Reconstitution After Transplant. *Sci Transl Med* (2017) 9(408). doi: 10.1126/scitranslmed.aan3085
32. Zeiser R, Blazar BR. Pathophysiology of Chronic Graft-Versus-Host Disease and Therapeutic Targets. *N Engl J Med* (2017) 377(26):2565–79. doi: 10.1056/NEJMra1703472
33. Hill GR, Betts BC, Tkachev V, Kean LS, Blazar BR. Current Concepts and Advances in Graft-Versus-Host Disease Immunology. *Annu Rev Immunol* (2021) 39:19–49. doi: 10.1146/annurev-immunol-102119-073227
34. Ara T, Hashimoto D. Novel Insights Into the Mechanism of GVHD-Induced Tissue Damage. *Front Immunol* (2021) 12:713631. doi: 10.3389/fimmu.2021.713631
35. Ichiba T, Teshima T, Kuick R, Misk DE, Liu C, Takada Y, et al. Early Changes in Gene Expression Profiles of Hepatic GVHD Uncovered by Oligonucleotide Microarrays. *Blood* (2003) 102(2):763–71. doi: 10.1182/blood-2002-09-2748
36. Giudicelli V, Duroux P, Ginestoux C, Folch G, Jabado-Michaloud J, Chaume D, et al. IMGT/LIGM-DB, the IMGT Comprehensive Database of Immunoglobulin and T Cell Receptor Nucleotide Sequences. *Nucleic Acids Res* (2006) 34(Database issue):D781–4. doi: 10.1093/nar/gkj088
37. Warren WC, Harris RA, Haukness M, Fiddes IT, Murali SC, Fernandes J, et al. Sequence Diversity Analyses of an Improved Rhesus Macaque Genome Enhance its Biomedical Utility. *Science* (2020) 370(6523). doi: 10.1126/science.abc6617
38. Luecken MD, Theis FJ. Current Best Practices in Single-Cell RNA-Seq Analysis: A Tutorial. *Mol Syst Biol* (2019) 15(6):e8746. doi: 10.15252/msb.20188746
39. Hafemeister C, Satija R. Normalization and Variance Stabilization of Single-Cell RNA-Seq Data Using Regularized Negative Binomial Regression. *Genome Biol* (2019) 20(1):296. doi: 10.1186/s13059-019-1874-1
40. Lane J, Duroux P, Lefranc MP. From IMGT-ONTOLOGY to IMGT/LIGMotif: The IMGT Standardized Approach for Immunoglobulin and T Cell Receptor Gene Identification and Description in Large Genomic Sequences. *BMC Bioinf* (2010) 11:223. doi: 10.1186/1471-2105-11-223
41. Turner SJ, Doherty PC, McCluskey J, Rossjohn J. Structural Determinants of T-Cell Receptor Bias in Immunity. *Nat Rev Immunol* (2006) 6(12):883–94. doi: 10.1038/nri1977
42. De Simone M, Rossetti G, Pagani M. Single Cell T Cell Receptor Sequencing: Techniques and Future Challenges. *Front Immunol* (2018) 9:1638. doi: 10.3389/fimmu.2018.01638
43. Han A, Glanville J, Hansmann L, Davis MM. Linking T-Cell Receptor Sequence to Functional Phenotype at the Single-Cell Level. *Nat Biotechnol* (2014) 32(7):684–92. doi: 10.1038/nbt.2938
44. Morris H, DeWolf S, Robins H, Sprangers B, LoCascio SA, Shonts BA, et al. Tracking Donor-Reactive T Cells: Evidence for Clonal Deletion in Tolerant Kidney Transplant Patients. *Sci Transl Med* (2015) 7(272):272ra10. doi: 10.1126/scitranslmed.3010760
45. Lindemann M. Ex Vivo Assessment of Cellular Immune Function - Applications in Patient Care and Clinical Studies. *Tissue Antigens* (2014) 84(5):439–49. doi: 10.1111/tan.12454
46. DeWolf S, Grinshpun B, Savage T, Lau SP, Obradovic A, Shonts B, et al. Quantifying Size and Diversity of the Human T Cell Alloresponse. *JCI Insight* (2018) 3(15). doi: 10.1172/jci.insight.121256
47. Zuber J, Shonts B, Lau SP, Obradovic A, Fu J, Yang S, et al. Bidirectional Intra-graft Alloreactivity Drives the Repopulation of Human Intestinal Allografts and Correlates With Clinical Outcome. *Sci Immunol* (2016) 1(4):doi: 10.1126/sciimmunol.aah3732
48. Rempala GA, Sewerny M. Methods for Diversity and Overlap Analysis in T-Cell Receptor Populations. *J Math Biol* (2013) 67(6-7):1339–68. doi: 10.1007/s00285-012-0589-7
49. Hutcheson K. A Test for Comparing Diversities Based on the Shannon Formula. *J Theor Biol* (1970) 29(1):151–4. doi: 10.1016/0022-5193(70)90124-4
50. Magurran AE. Biological Diversity. *Curr Biol* (2005) 15(4):R116–8. doi: 10.1016/j.cub.2005.02.006

51. Kanehisa M, Goto S. KEGG: Kyoto Encyclopedia of Genes and Genomes. *Nucleic Acids Res* (2000) 28(1):27–30. doi: 10.1093/nar/28.1.27
52. Graubert TA, Russell JH, Ley TJ. The Role of Granzyme B in Murine Models of Acute Graft-Versus-Host Disease and Graft Rejection. *Blood* (1996) 87(4):1232–7. doi: 10.1182/blood.V87.4.1232.bloodjournal8741232
53. DeTomaso D, Jones MG, Subramaniam M, Ashuach T, Ye CJ, Yosef N. Functional Interpretation of Single Cell Similarity Maps. *Nat Commun* (2019) 10(1):4376. doi: 10.1038/s41467-019-12235-0
54. Joshi K, Milighetti M, Chain BM. Application of T Cell Receptor (TCR) Repertoire Analysis for the Advancement of Cancer Immunotherapy. *Curr Opin Immunol* (2021) 74:1–8. doi: 10.1016/j.coi.2021.07.006
55. Smith C, Corvino D, Beagley L, Rehan S, Neller MA, Crooks P, et al. T Cell Repertoire Remodeling Following Post-Transplant T Cell Therapy Coincides With Clinical Response. *J Clin Invest* (2019) 129(11):5020–32. doi: 10.1172/JCI128323
56. Nikolich-Zugich J, Slika MK, Messaoudi I. The Many Important Facets of T-Cell Repertoire Diversity. *Nat Rev Immunol* (2004) 4(2):123–32. doi: 10.1038/nri1292
57. Babel N, Stervbo U, Reinke P, Volk HD. The Identity Card of T Cells-Clinical Utility of T-Cell Receptor Repertoire Analysis in Transplantation. *Transplantation* (2019) 103(8):1544–55. doi: 10.1097/TP.0000000000002776
58. Meier JA, Haque M, Fawaz M, Abdeen H, Coffey D, Towler A, et al. T Cell Repertoire Evolution After Allogeneic Bone Marrow Transplantation: An Organizational Perspective. *Biol Blood Marrow Transplant* (2019) 25(5):868–82. doi: 10.1016/j.bbmt.2019.01.021
59. Brochu HN, Tseng E, Smith E, Thomas MJ, Jones AM, Diveley KR, et al. Systematic Profiling of Full-Length Ig and TCR Repertoire Diversity in Rhesus Macaque Through Long Read Transcriptome Sequencing. *J Immunol* (2020) 204(12):3434–44. doi: 10.4049/jimmunol.1901256
60. Rosenfeld R, Zvi A, Winter E, Hope R, Israeli O, Mazor O, et al. A Primer Set for Comprehensive Amplification of V-Genes From Rhesus Macaque Origin Based on Repertoire Sequencing. *J Immunol Methods* (2019) 465:67–71. doi: 10.1016/j.jim.2018.11.011
61. Li Z, Liu G, Tong Y, Zhang M, Xu Y, Qin L, et al. Comprehensive Analysis of the T-Cell Receptor Beta Chain Gene in Rhesus Monkey by High Throughput Sequencing. *Sci Rep* (2015) 5:10092. doi: 10.1038/srep10092
62. Ma S, Zhang B, LaFave LM, Earl AS, Chiang Z, Hu Y, et al. Chromatin Potential Identified by Shared Single-Cell Profiling of RNA and Chromatin. *Cell* (2020) 183(4):1103–16 e20. doi: 10.1016/j.cell.2020.09.056
63. Angermueller C, Clark SJ, Lee HJ, Macaulay IC, Teng MJ, Hu TX, et al. Parallel Single-Cell Sequencing Links Transcriptional and Epigenetic Heterogeneity. *Nat Methods* (2016) 13(3):229–32. doi: 10.1038/nmeth.3728

**Conflict of Interest:** AS reports compensation for consulting and/or SAB membership from Merck, Honeycomb Biotechnologies, Cellarity, Repertoire Immune Medicines, Hovione, Third Rock Ventures, Ochre Bio, FL82, and Dahlia Biosciences unrelated to this work. AS has received research support from Merck, Novartis, Leo Pharma, Janssen, the Bill and Melinda Gates Foundation, the Moore Foundation, the Pew-Stewart Trust, Foundation MIT, the Chan Zuckerberg Initiative, Novo Nordisk and the FDA unrelated to this work. LK is on the scientific advisory board for HiFiBio and Mammoth Biosciences. She reports research funding from Kymab Limited, Magenta Therapeutics, BlueBird Bio, and Regeneron Pharmaceuticals. She reports consulting fees from Equillium, FortySeven Inc, Novartis Inc, EMD Serono, Gilead Sciences, Vertex Pharmaceuticals, and Takeda Pharmaceuticals. LK reports grants and personal fees from Bristol Myers Squibb that are managed under an agreement with Harvard Medical School.

The remaining authors declare that the research was conducted in the absence of any commercial or financial relationships that could be construed as a potential conflict of interest.

**Publisher's Note:** All claims expressed in this article are solely those of the authors and do not necessarily represent those of their affiliated organizations, or those of the publisher, the editors and the reviewers. Any product that may be evaluated in this article, or claim that may be made by its manufacturer, is not guaranteed or endorsed by the publisher.

Copyright © 2022 Gerdemann, Fleming, Kaminski, McGuckin, Rui, Lane, Keskula, Cagnin, Shalek, Tkachev and Kean. This is an open-access article distributed under the terms of the Creative Commons Attribution License (CC BY). The use, distribution or reproduction in other forums is permitted, provided the original author(s) and the copyright owner(s) are credited and that the original publication in this journal is cited, in accordance with accepted academic practice. No use, distribution or reproduction is permitted which does not comply with these terms.